Inorganic Chemistry

pubs.acs.org/IC Article

Bisaryl and Bisalkynyl Diruthenium (III,III) Compounds Based on an Electron-Deficient Building Block

Lyndsy A. Miller-Clark, Peter E. Christ, Brian T. Barbarini, and Tong Ren*



Cite This: Inorg. Chem. 2022, 61, 14871-14879



Read Online

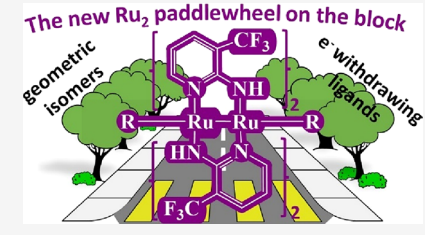
ACCESS

III Metrics & More

Article Recommendations

Supporting Information

ABSTRACT: Reported herein is a new series of diruthenium(III,III) bisalkynyl and bisaryl diruthenium(III,III) compounds supported with 2-amino-3-(trifluoromethyl)-pyridinate (amtfmp). Using Ru₂(amtfmp)₄Cl₂ from a modified preparation, *cis* 2:2 Ru₂(amtfmp)₄(Ph)₂ (2), and 3:1 Ru₂(amtfmp)₄(Ph)₂ (3) were synthesized via a lithium-halogen exchange reaction using LiC₂Ph and LiPh, respectively. Compounds 1–3 are all Ru₂(III,III) species with a ground-state configuration of $\pi^4\delta^2(\pi^*)^4$ (S=0) and were characterized via mass spectrometry, electron absorption and $^1H/^{19}F$ NMR spectroscopies, and voltammetry. The molecular structures of 1–3 were established using single-crystal X-ray diffraction analysis,



and preliminary density functional theory analysis was performed to elaborate the electronic structures of 1 and 2. Comparisons of the electrochemical properties of 1-3 against the $Ru_2(amtfmp)_4Cl_2$ starting material reveal cathodic shifts of the $Ru_2^{7+/6+}$ oxidation and the $Ru_2^{6+/5+}$ and $Ru_2^{5+/4+}$ reduction potentials. In comparison to related $Ru_2(III,III)$ bisalkynyl and bisaryl compounds, the electrode potentials for 1-3 are anodically shifted up to ca. 0.95 V, highlighting the strong electron-withdrawing nature of the amtfmp ligand.

■ INTRODUCTION

Since the discovery of diruthenium(II,III) tetracarboxylates by Wilkinson and co-workers, ¹ the chemistry of diruthenium paddlewheel compounds of the form $[Ru_2(L)_4X_n]$ (L= bridging ligands, X= axial ligands; n=0,1,2) has flourished. ^{2,3} A common characteristic of diruthenium compounds is their rich redox properties and a large range of accessible oxidation states from $Ru_2(I,II)$ to $Ru_2(III,IV)$, which has recently been detailed in a review by Kadish and co-workers. ⁴ Diruthenium-(II,III) species are often of a S=3/2 ground state, and these compounds have been used as the building blocks for magnetic materials with pioneering contributions from the laboratories of Handa, ^{5,6} Miller, ^{7,8} Dunbar, ⁹ and Jiménez-Aparicio. ^{10,11} Aerobic and peroxy oxidation catalysis by diruthenium species is another interesting development in recent years. ^{12–15}

Many examples of Ru₂ organometallic compounds have been disclosed since the seminal report of Ru₂(ap)₄(C_2 Ph) (ap = 2-anilinopyridinate) by Cotton and Chakravarty¹⁶ and subsequent studies by Bear and Kadish.^{17,18} Ru₂(ap)₄-based compounds are highly robust both under ambient conditions and over a broad electrochemical window, and spectroelectrochemistry studies of the Ru₂(ap)-bridge-Ru₂(ap) type compounds have provided clear evidence for facile charge delocalization across oligoynyl (bridge = C_{2n})^{19–22} and aryl (bridge = C_6 H₄) bridges.²³ The chemical robustness of Ru₂(ap)₄-based compounds also allows for iterative oncomplex Cadiot—Chodkiewicz coupling, yielding extended oligo-yne compounds Ru₂(ap)₄(C_{2k} SiR₃) with k up to 5.²⁴ The ability to mediate charge transfer has been exploited in the construct of prototypical molecular wires²⁵ and devices.^{26–28}

Recent work by the laboratory of Akita further illustrates the unique conductivity characteristics afforded by the tunable valence orbital distribution of Ru_2 alkynyls near the Fermi level of the nanojunction. In addition to $\mathrm{Ru}_2(ap)_4$ -based organometallics, assemblies based on $\mathrm{Ru}_2(ap)_4(\mathrm{CN})$ have been utilized for studying spin-coupling and metal—metal charge-transfer transitions by the laboratory of Sheng in recent years. Addish and Van Caemelbecke investigated the formation of water-soluble $\mathrm{Ru}_2(\mathrm{OAc})_3(\mathrm{L})\mathrm{Cl}$ with L as a variety of fluorinated ap ligands.

In addition to ap and its fluorinated analogues, two other types of bridging ligands, DArF (DArF = N,N'-diary-lformamidinate, Scheme 1) and DMBA (DMBA = N,N'-dimethylbenzamidinate), have been frequently employed to support Ru₂(III,III) organometallic compounds. $^{17,34-37}$ While bisalkynyls Ru₂(III,III) are attainable with all three types of ligands, the steric requirements enforced by the bridging ligands' flanking phenyls 38,39 has resulted in bisaryls Ru₂(III,III) only being achieved with DMBA thus far. 40 Hence, the arrangement of dissymmetric N,N'-bidentate ligands around the Ru₂ core, Scheme 1, is significant in dictating the number of aryl ligands at the axial positions.

Received: July 14, 2022 Published: September 9, 2022





Scheme 1. (a) Symmetric and Asymmetric N,N' Bridging Ligands and (b) Possible Configurations of Ru₂ Compounds $(Y = -Cl, -C \equiv C, \text{ and } -Ar)$

In recent years, Kataoka et al. have developed several Ru₂(III,III) dichloro compounds based on less bulky bridging ligands including benzamidinate, 41 2-aminopyridinate (amp) and 2-amino-4-methylpyridinate, 42 and 2-amino-3-(trifluoromethyl)pyridinate (amtfmp). 43 All Ru₂(III,III) dichloro compounds based on 2-aminopyridinate-type ligands adopted a cis 2:2 arrangement, despite the multiple possible configurations shown in Scheme 1. 42,43 Among the many interesting attributes reported for Ru₂(amtfmp)₄Cl₂ are its drastic electrochromism in the NIR window and a high degree of electron deficiency evidenced by a very anodic Ru₂+6/+5 couple (0.36 V vs the saturated calomel electrode).⁴³ Intrigued by the impact of organometallic derivatization on such an electron-poor Ru, building block, we have explored both the alkynylation and arylation at the axial positions of Ru₂(amtfmp)₄Cl₂, and the details of synthesis and structural and voltammetric characterizations are reported here.

RESULTS AND DISCUSSION

Synthesis. In the original report by Kataoka, Ru₂(amtfmp)₄Cl₂ was prepared from refluxing Ru₂(OAc)₄Cl with Hamtfmp in THF/Et₃N, with a yield of 54%. 43 Aiming to increase the yield, we prepared Ru₂(amtfmp)₄Cl₂ using a protocol developed for Ru₂(ap)₄Cl: refluxing Ru₂(OAc)₄Cl with 8 equiv of Hamtfmp and LiCl in excess, while the condenser was outfit with a micro-Soxhlet extractor containing K_2CO_3 to drive the reaction. Ru₂(amtfmp)₄Cl₂ was obtained as a deep-blue solid in a yield (55%) comparable to the original report 43 after purification. Thin-layer chromatography (TLC) with 1:2 THF/hexanes with 3% MeOH (v/v) revealed the presence of two isomers with very similar R_f values $(R_{\rm f}=0.30,\ 0.33)$ in the purified material (Figure S18). It is likely that the higher reaction temperature achieved in refluxing toluene enabled the formation of the two different isomers instead of just the cis 2:2 isomer reported by Kataoka. 42,43 Furthermore, Ru₂(amtfmp)₄Cl₂ prepared using the Kataoka protocol in our laboratory comprised two isomers as well (see the Supporting Information, pp S20-S23). Previously, Bear and Kadish's molten syntheses (>120 °C) of $Ru_2(F_xap)_4Cl$ (x = 2, 3) produced a mixture of the (4,0) and (3,1) isomers regardless of the reaction length. ^{47,48} The lability of both fluorinated and unfluorinated anilinopyridinate ligands has also been observed upon reaction with CN^- , Cl^- , or $-C\equiv$ CC₅H₄N. ^{49,50} In the case of CN⁻, the coordination mode could be controlled via reaction temperature, resulting in the rearrangement of two F₅ap ligands to facilitate a CN⁻ ligand that is σ -bonded to one Ru atom and π -bonded to the other Ru over axial coordination.⁵⁰ While attempts to crystallize the 3:1 isomer of Ru₂(amtfmp)₄Cl₂ have failed thus far, ¹⁹F NMR confirmed the presence of a small amount of the 3:1 isomer in the purified material (Figure S4).

As shown in Scheme 2, the bisalkynyl $Ru_2(amtfmp)_4(C \equiv CPh)_2$ (1) and bisaryl $Ru_2(amtfmp)_4(Ph)_2$ were prepared from the reaction of $Ru_2(amtfmp)_4Cl_2$ with excess LiC_2Ph or LiPh. 35,40 The cis 2:2 $Ru_2(amtfmp)_4(C \equiv CPh)_2$ isomer (1) was isolated as a blue—green solid (36% based on Ru_2) and structurally identified (see below), while the corresponding 3:1 bisalkynyl isomer was not isolated in spite of the presence of a 3:1 isomer in the starting material. From the analogous LiPh reaction, a crude bisaryl product was isolated in 33% yield (based on Ru_2) after a silica plug purification, which is a mixture of a deep-red species [$R_f = 0.73$, 1:2 THF/hexanes w/

Scheme 2. Synthetic Approach to Produce $Ru_2(amtfmp)_4(Y)_2$ (Y = C_2Ph , Ph) Compounds 1–3

3% MeOH (v/v)] and a purple species [$R_f = 0.70$, 1:2 THF/hexanes w/3% MeOH (v/v)]. Careful silica column purification (1:2 THF/hexanes w/3% MeOH) yielded a clean red fraction (2, 12%) and a purple fraction (3, 7%), which were unambiguously identified, respectively, as the *cis* 2:2 and 3:1 isomers using crystallography (see below). The low (combined) yields of compounds 1–3 are likely attributed to the in situ reduction of $Ru_2(amtfmp)_4Cl_2$ by organo-lithium species. A large quantity of red baseline species is always present in all of the above-mentioned reactions (Figure S19), and its absorption spectrum (Figure S9) matches that reported for $[Ru_2(amtfmp)_4Cl_2]^{-1}$. The red solid can be converted to the starting materials $Ru_2(amtfmp)_4Cl_2$ via reoxidation upon exposure to air as a suspension in CH_2Cl_2 in *ca.* 40% yield.

Upon isolation, compounds 1-3 are relatively stable both as solids and in solution in ambient conditions, with 1 degrading to intractable products within a week and 2 and 3 stable for over a month. Like the related $Ru_2(III,III)$ bisalkynyl/bisaryl compounds based on $Ru_2(DMBA)_{4}^{35,40}$ compounds 1-3 are diamagnetic, enabling characterization via ¹H and ¹⁹F NMR spectroscopy. With an effective C_{2h} symmetry, the four amtfmp ligands in both 1 and 2 are equivalent, and hence, there is only one fluorine peak (Figures S5 and S6). The 3:1 arrangement of amtfmp in 3 resulted in three fluorine peaks, one double the intensity of the other two (Figure S7), confirming that one set of trans amtfmp ligands experience similar environments, while the other set of trans ligands are in different environments. Further characterization of 1-3 was achieved using electrospray mass spectroscopy (ESI-MS), vis-NIR, and FT-IR (in the case of 1, Figure S8) spectroscopies, cyclic (CV) and differential pulse voltammetry (DPV), single-crystal X-ray diffraction studies, and combustion analysis.

Molecular Structures. Molecular structures of compounds 1, 2, and 3 have been determined using single-crystal X-ray diffraction, as shown in Figures 1, 2, and 3, respectively, and

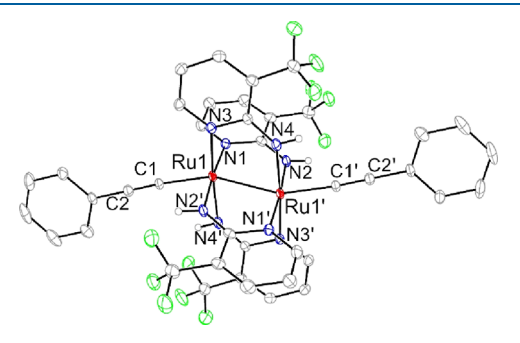


Figure 1. ORTEP plot of 1 at a 30% probability level, with most H atoms omitted for clarity.

selected bond lengths are given in Table 1. In 1 and 2, the bridging amtfmp ligands adopt a *cis* 2:2 arrangement around the Ru₂ unit and both structures contain a crystallographic inversion center in the midpoint of the Ru–Ru bond. Compound 3 contains three bridging amtfmp ligands in the same orientation with the fourth ligand opposite, resulting in a C_1 symmetry. The Ru–Ru bond lengths for 1 (2.4656(4) Å), 2 (2.5144[4] Å), and 3 (2.5035(4) Å) are all significantly lengthened when compared to Ru₂(amtfmp)₄Cl₂ (2.330[2] Å), highlighting the weakening of the σ (Ru–Ru) bond by the strong electron donation from the alkynyl and aryl ligands. The Ru–Ru bond length for 1 is a close match to Ru₂(DMBA)₄(C≡CR)₂ (avg. 2.45 Å), s5,51 but the Ru–Ru

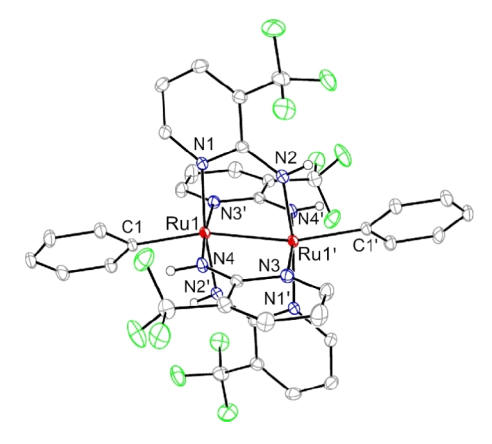


Figure 2. ORTEP plot of 2 at a 30% probability level, with most H atoms omitted for clarity.

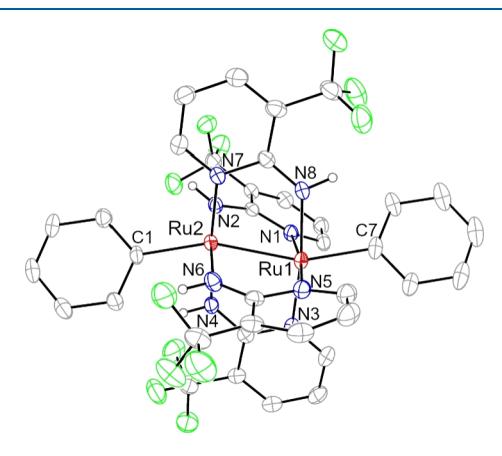


Figure 3. ORTEP plot of 3 at a 30% probability level, with most H atoms omitted for clarity.

Table 1. Selected Bond Lengths (Å) and Angles (deg) for 1-3

	1	2 ^a	3
Ru1-Ru2	2.4656(4)	2.5144[4]	2.5036(4)
Ru-C	1.979(3)	2.047[3]	2.040(4)/2.070(4)
C1-C2	1.203(4)		
Ru1'-Ru1-C1	157.23(8)	158.60[8]	159.3[1]
Ru1-N1	2.026(2)	2.032(2)	2.148(5)
Ru1-N3	2.058(2)	2.060(2)	2.072(4)
Ru1-N4		2.008(2)	
Ru1-N5			2.071(4)
Ru1-N8			2.035(5)
Ru2(Ru1')-N2	2.051(3)	2.063(2)	1.981(6)
Ru2(Ru1')-N4	2.021(2)		2.046(3)
Ru2(Ru1')-N5		2.041(2)	
Ru2(Ru1')-N6		2.045(2)	2.040(3)
Ru2(Ru1')-N7		2.062(2)	2.069(5)
Ru2(Ru1')-N8		2.012(2)	

^aAveraged over two independent molecules.

bond lengths are slightly lengthened for 2 and 3 when compared to other $Ru_2(III,III)$ σ -aryl compounds $(Ru_2(DMBA)_4(Ar)_2$: avg. 2.4989 Å).

The averaged Ru–C bond lengths for 2 (2.047[3] Å) and 3 (2.055[5] Å) are significantly longer than that of 1 (1.979(3) Å), matching the trend from previous comparisons between either aryl $Ru_2(II,III)^{39}$ or bisaryl $Ru_2(III,III)^{40}$ compounds

and their alkynyl or bisalkynyl counterparts. Again, the Ru–C bond length of 1 is a good match when compared to Ru₂(DMBA)₄(C \equiv CR)₂ compounds (avg. 1.97 Å), 35,51 while 2 and 3 are slightly shortened when compared to Ru₂(DMBA)₄(Ar)₂ compounds (avg. 2.071 Å), 40 complementing the increased Ru–Ru bond lengths discussed above. This suggests a more robust engagement of the Ru d_z² orbitals by the stronger σ -donating Ar⁻ ligands, forming slightly stronger Ru–C σ bonds. 40

Compounds 1-3 exhibit significant distortions from an idealized paddlewheel geometry, as highlighted by the large deviation of Ru-Ru-C from linearity (avg. 158°, Table 1). The distortion observed in compounds 1-3 is attributed to a second-order Jahn-Teller (SOJT) effect. Thorough documentation and analysis of this effect has been described elsewhere for related Ru₂(III,III)L₄X₂-type compounds, 52 including the Ru₂(DMBA)₄(C \equiv CR)₂ 35,51,53 and Ru₂(DMBA)₄(Ar)₂ compounds.⁴⁰ Of note are the analogous $Ru_2(III,III)$ σ -alkynyl compounds, such as $Ru_2(DMBA)_4(C \equiv CR)_2^{35,53}$ (Ru-Ru-C ranges between 161 and 175°), which do not present as significant distortions as observed in 1. The partially repressed SOJT effect in $Ru_2(DMBA)_4(C \equiv CR)_2$ has been attributed to steric repulsion between the alkynyl substituents and the N-Me groups,⁵² a repulsion not achievable with the amino protons in amtfmp. The related $Ru_2(DMBA)_4(Ar)_2$ complexes, however, also present significant structural distortions (Ru-Ru-C: avg. 152°). 40 The relatively narrow range of the Ru-Ru-C angle among 1-3 is plausibly related to the electronic structure instead of sterics: the angle is optimized to rotate the Ru d π orbitals in the formally $\pi^*(Ru-Ru)$ [HOMO – 2, see density functional theory (DFT) discussion below] for a strong σ -bonding interaction.⁴⁴

Electronic Absorption Spectra. The vis–NIR absorption spectra of compounds 1–3 and Ru₂(amtfmp)₄Cl₂ recorded as THF solutions are shown in Figure 4. Ru₂(amtfmp)₄Cl₂ is

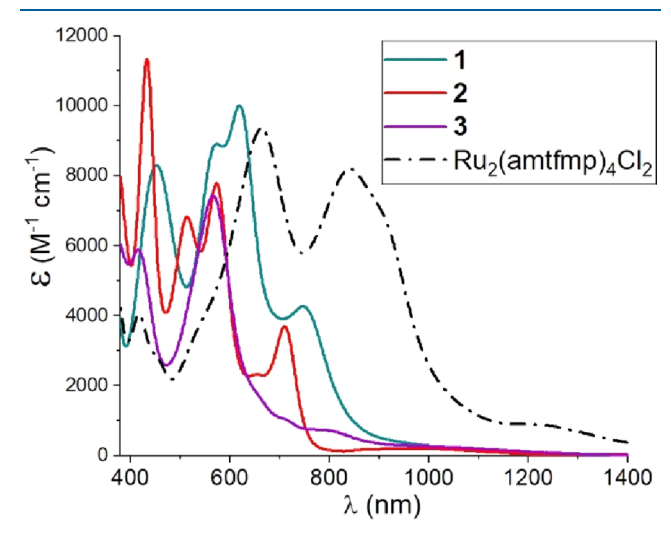


Figure 4. Vis–NIR absorption spectra of 1–3 and ${\rm Ru_2(amtfmp)_4Cl_2}$ in THF.

deeply colored, and its absorption spectrum is dominated by intense metal charge-transfer transition (LMCT; ⁴³ see DFT discussion below) bands at 660 and 845 nm. Upon alkynylation, the LMCT bands of 1 were blue-shifted from that of $Ru_2(amtfmp)_4Cl_2$ and split into four bands. Arylation of diruthenium further blue-shifts the LMCT bands in 2 and 3,

and a satellite band appears next to the lowest energy LMCT band in 2 (656 nm) as well. In the case of 3, only two intense visible transitions are observed (415 and 566 nm), aligning reasonably with two of the transitions in 2 (433 and 573 nm). Less intense transitions ($\leq 1000~\text{M}^{-1}~\text{cm}^{-1}$) at lower energies (710 and 800 nm) in 3 can also be observed, presumably of reduced intensities due to the lower symmetry of 3 compared to 2. Compounds 2 and 3 also exhibit a weak and broad band between 800 and 1100 nm, while such a band is not obvious in 1, likely obscured by the LMCT band. The low intensity (<300 M⁻¹ cm⁻¹) indicates that this transition is primarily localized on the Ru₂ core, similar to the case of Ru₂(DMBA)₄(Ar)₂.⁴⁰

Electrochemical Studies. The redox properties of 1-3 were examined using CV and DPV. The voltammograms of 1-3 are plotted in Figure 5, with an isomeric mix of $Ru_2(amtfmp)_4Cl_2$ and pure cis 2:2 $Ru_2(amtfmp)_4Cl_2$ plotted in Figure S11. The respective redox potentials for 1-3 are listed in Table 2.

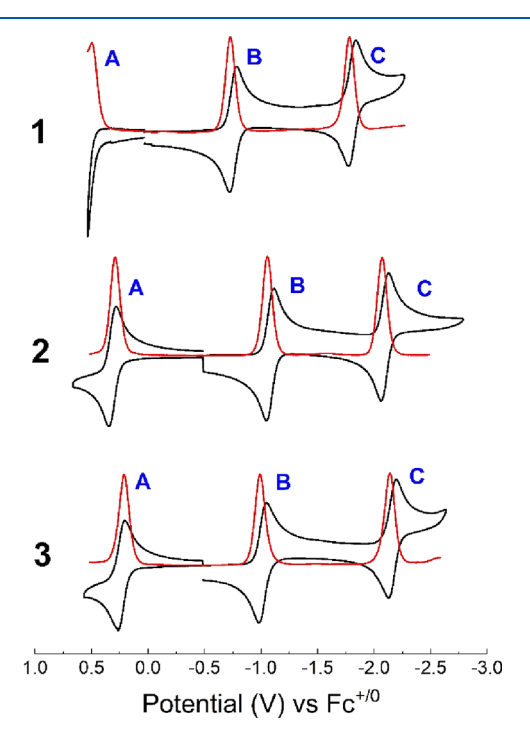


Figure 5. Cyclic (black) and differential pulse (red) voltammograms of compounds 1-3 (1.0 mM) recorded in 0.10 M THF solutions of $\mathrm{Bu_4NPF_6}$ at a scan rate of 0.10 V s⁻¹.

All compounds exhibit two reversible reductions, **B** (Ru₂^{6+/5+}) at -0.75 (1), -1.08 (2), and -1.01 V (3) (vs Fc^{+/0}) respectively, and C (Ru₂^{5+/4+}) at -1.81 V (1), -2.10 (2), and -2.16 V (3). Compounds 2 and 3 both exhibit one reversible oxidation **A** (Ru₂^{7+/6+}) at 0.31 (2) and 0.24 V (3);

Table 2. Electrode Potentials (in V vs $Fc^{+/0}$) for $Ru_2(amtfmp)_4(Y)_2$ in THF

Y	A	В	C
$-C_2Ph(1)$	0.62 ^a	-0.75	-1.81
-Ph (2)	0.31	-1.08	-2.10
-Ph (3)	0.24	-1.01	-2.16
-Cl		-0.17	-1.59

^aOnly partially visible in DPV, no obvious peak in CV.

however, a peak potentially corresponding to an analogous, irreversible peak A is visible at *ca.* 0.60 V (at the edge of the potential window allowed in THF) in the DPV of 1 (Figure S12). The cathodically shifted oxidation and reduction potentials in 2 and 3 highlight the aryl ligand being a stronger electron donor than both chloro and alkynyl ligands (see discussion above). Both reductions B and C for compounds 1–3 are cathodically shifted from the dichloro starting material (Figure S11 and Table S3).⁴³ The couple B is shifted by ca. –0.88 V for the bisaryl compounds 2 and 3 but only shifted by –0.57 V for 1. The couple C is only shifted by ca. –0.43 V for 1–3 when compared to Ru₂(amtfmp)₄Cl₂.

The contrast in electrode potentials between 2 and 3 is different from that reported for (4,0), (3,1), and (2,2)-trans geometric isomers of $Ru_2(F_5ap)_4Cl$ (F_5ap = pentafluoroanilinopyridinate). All geometric isomers of $Ru_2(F_5ap)_4Cl$ exhibited reversible $Ru_2^{5+/4+}$, $Ru_2^{6+/5+}$, and $Ru_2^{7+/6+}$ redox processes, all of which were sensitive to the type of regioisomer that was being studied. All processes cathodically shifted by at least 0.10 V when comparing the (4,0) processes to either the (3,1) or the (2,2)-trans isomers. 48 When comparing the redox events of 2 and 3, a similar cathodic shift of at least 0.06 V is observed in the oxidation A $(Ru_2^{7+/6+})$ and the second reduction C (Ru₂^{5+/4+}). However, the first reduction B $(Ru_2^{6+/5+})$, which is proposed to occur on the LUMO of the two compounds, for 3 is anodically shifted by 0.07 V from that of 2. Presumably, the LUMO of the two compounds comprises differing δ^*/π^* orbitals, generated through the differing bond requirements of the isomers. This contrasts with previous studies on the (4,0) and (3,1) $Ru_2(F_xap)_4Cl(x = 1-3)^{47}$ and $Ru_2(F_xap)_4(C_2Ph)_2(x = 1, 2, 5)^{54}$ isomers: these demonstrated that the highest filled orbital (first oxidation event), either δ^* (-Cl) or π^* ((-C₂Ph)₂), is more sensitive to isomer type than the lowest unoccupied orbitals (first reduction event).

When the electrode potentials of 1 are compared to $Ru_2(DMBA)_4(C_2Ph)_2^{35}$ there is an approximate 0.85 V anodic shift of both reduction events B and C (Table S3), highlighting the strong electron-withdrawing nature of amtfmp. With respect to $Ru_2(DMBA)_4(Ph)_2$, compounds 2 and 3 also exhibit anodic shifts of events A and B: 0.74 V for A and 0.94 V for B (Table S3). The second reduction event is irreversible in $Ru_2(DMBA)_4(Ph)_2$ due to the dissociation of a Ph^{-40} but is perfectly reversible in 2 and 3, which indicates the remarkable stability of $[Ru_2(amtfmp)_4(Ph)_2]^{2-}$.

DFT Calculations on 1 and 2. DFT calculations were also performed to better understand the electronic structures of 1 and 2. Representations of the Frontier molecular orbitals and their corresponding energies for 1' and 2' are shown in Figure 6 and Table S4, and the comparison between experimental (crystallographic) and DFT-optimized parameters is given in Table S5. Computational details can be found in the Supporting Information.

It is clear from Figure 6 that the Frontier molecular orbitals of both 1' and 2' are heavily mixed between the Ru₂ core and the bisalkynyl (1') and bisaryl (2') ligands. As postulated in the voltammetric studies above, the HOMO of 2' is mainly based on $d\pi^*$ interactions within the Ru₂ core with some limited ligand interaction, analogous to the previously characterized Ru₂(DMBA)₄(Ar)₂. In contrast, the HOMO of 1' is mainly the antibonding $d\pi$ (Ru₂) $-\pi$ (C \equiv C-Ph) combination, consistent with the acetylide ligand being a π -base. For both 1' and 2', the HOMO – 2 orbital has gained

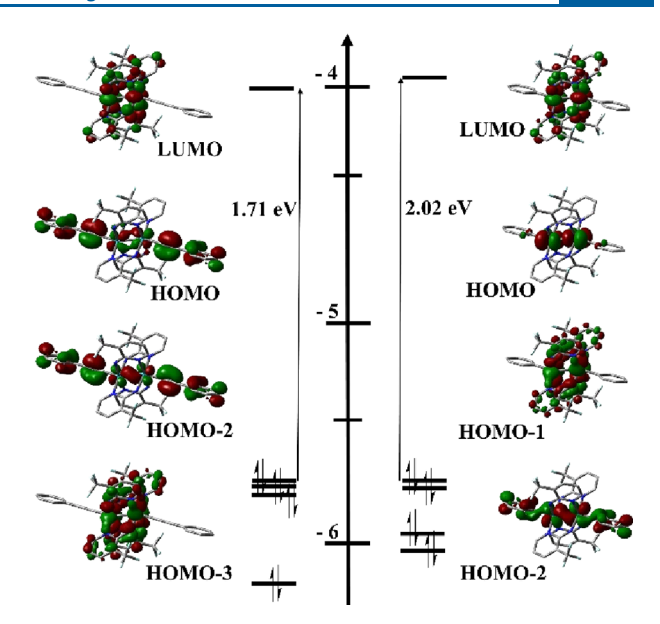


Figure 6. Molecular orbital diagrams of 1' (left) and 2' (right) obtained from DFT calculations, represented at lisovaluel = 0.03. The HOMO – 1 for 1' was omitted as it consists of the $d\pi-\pi$ interactions akin to the HOMO of 1' but in the orthogonal orientation (plotted in Table S4).

some $\sigma(Ru-Ru)$ character via the SOJT distortion, which is caused by large deviations from linearity in the Ru-Ru-C bond angles. Around this orbital, both a $\delta(Ru_2)/\pi(Ru-N)$ orbital (HOMO - 1) and a $\pi(Ru-Ru)/\pi(Ru-Ar)$ orbital (HOMO - 3) can also be found. While 1' does contain the analogous orbitals, they are found in a slightly different order, with only the HOMO - 2 and LUMO matching the order for 2'. The LUMO and higher-energy orbitals in both 1' and 2' are localized on the $\delta^*(Ru_2)$ orbitals (Table S4) with some nonbonding $\pi(N-C-N)$ amtfmp ligand contributions, suggesting that the reductions observed in voltammetric studies (see discussion above) are also primarily based on the Ru₂ core. Thus, the overall ground-state configurations of 1' and 2' (and presumably 3, based on diamagnetic ¹H NMR) can be represented as $\pi^4 \delta^2(\pi^*)^4$ (S = 0), matching the previously characterized $Ru_2(DMBA)_4(Ar)_2$ and $Ru_2(DMBA)_4(C_2R)_2$ compounds. 35,36,40

CONCLUSIONS

Preparation of organometallic derivatives of $Ru_2(amtfmp)_4Cl_2$ has been successfully demonstrated in this study. Both the bisalkynyl (1) and bisaryl (2 and 3) derivatives exhibit multiple reversible one-electron couples and are rich in colors, revealing their potential for applications as charge storage and electrochromic materials. In spite of the contrast in electron donicity between DMBA and amtfmp, $Ru_2(amtfmp)_4(Y)_2$ compounds are iso-electronic to the corresponding $Ru_2(DMBA)_4(Y)_2$ (Y = Cl, C_2Ph or Ph). A severe setback from a synthesis perspective is that all $Ru_2(amtfmp)_4(Y)_2$ materials obtained by us are mixtures of cis 2:2 and 3:1 isomers, a reflection of the substitution lability of the amtfmp ligand. Preparing $Ru_2(amtfmp)_4(Y)_2$ of both good isomeric purity and respectable yield is a bottleneck toward material applications and an ongoing effort in our laboratory.

■ EXPERIMENTAL SECTION

General Information. $\mathrm{Ru}_2(\mathrm{OAc})_4\mathrm{Cl}$ was prepared according to a previously reported method. ¹ "BuLi (2.5 M in hexanes) was purchased from Sigma-Aldrich. 2-Amino-3-(trifluoromethyl)pyridine, phenylacetylene, and bromobenzene were purchased from Oakwood Chemicals and used without further purification. Tetrahydrofuran (THF) was freshly distilled over sodium/benzophenone. All reactions were performed under a dry nitrogen atmosphere implementing standard Schlenk procedures unless otherwise noted, with workups occurring in ambient conditions.

Physical Methods. UV-vis-NIR spectra were obtained using a JASCO V-780 spectrophotometer in THF solutions. The FT-IR spectrum of 1 was measured as a neat sample using a JASCO FT/IR-6300 spectrometer equipped with a diamond ATR attachment. ESI-MS were analyzed on an Advion mass spectrometer. ¹H and ¹⁹F NMR spectra were recorded using a Varian Inova 300 spectrometer operating at 300 MHz (¹H) and 282 MHz (¹⁹F). Cyclic and differential pulse voltammograms were recorded in a 0.1 M ("Bu₄N)PF₆ solution (4 mL of THF, Ar-degassed) on a CHI620A voltammetric analyzer with a glassy carbon working electrode (diameter 2 mm), a Pt-wire auxiliary electrode, and a Ag/AgCl reference electrode. The concentration of Ru₂ species was always ca. 1.0 mM. The Fc^{+/0} couple was observed at ca. 0.480 \pm 0.011 V (vs Ag/AgCl) under the noted experimental conditions. Elemental analyses were performed by Atlantic Microlab, Inc. Magnetic susceptibility of Ru₂(amtfmp)₄Cl₂ was measured using a Johnson Matthey MarkII magnetic susceptibility balance at 294 ± 2 K.

Synthesis. Ru₂(amtfmp)₄Cl₂. To a 100 mL round-bottom flask were added Ru₂(OAc)₄Cl (240 mg, 0.50 mmol), 2-amino-3-(trifluoromethyl)pyridine (650 mg, 4.0 mmol), excess LiCl (300 mg, 7.0 mmol), and 60 mL toluene, and a micro-Soxhlet extraction apparatus with a K2CO3-filled glass thimble was mounted atop the flask. The reaction mixture was then refluxed at ca. 130 °C for a week, with K2CO3 changed daily for the first 3 days, and then once after. After cooling to room temperature, the deep-blue crude mixture was filtered over Celite and the remaining solid was washed with methanol. All fractions were combined, and after solvent removal, the residue was dissolved in CH2Cl2, exposed to air to reoxidize after reduction from methanol exposure, and filtered once TLC confirmed product presence (usually 2-3 days). This was repeated over the course of 2 weeks until no more product was identified via TLC. The deep-blue filtrate was dried to a dark solid, while any remaining residue was washed with methanol, condensed, and redissolved in CH2Cl2. Final purification of the deep-blue filtrate was achieved by running a CH₂Cl₂ (0-5% methanol) silica plug. Yield: 255 mg Ru₂(amtfmp)₄Cl₂ (55% yield based on Ru). Ru₂(amtfmp)₄Cl₂ was recrystallized in a 1:25 THF/hexanes (v/v) before EA. TLC with 1:2 THF/hexanes with 3% methanol (v/v) revealed the presence of two blue spots, $R_f = 0.33$; 0.30. Elem. Anal. Found (calcd) for $C_{28}H_{24}N_8O_1F_{12}Cl_2Ru_2$ (Ru₂(amtfmp)₄Cl₂·1THF): C, 33.88 (33.98); H, 2.17 (2.44); N, 11.75 (11.32). ESI-MS (m/z, based on 101Ru): $[M]^- = 918.3$. UV-Vis (in THF) λ/nm (ε/M^{-1} cm⁻¹): 662 (9400), 843 (8200), 1200 (900). Electrochemistry (THF, vs Fc^{+/0}) $E_{1/2}/V$, $\Delta E_{\rm p}/{\rm mV}$, $i_{\rm backward}/i_{\rm forward}$: -0.168 (66, 0.98), -1.591 (71, 0.83). $\mu_{\rm eff}$: 2.71 $\mu_{\rm B}$. ¹⁹F NMR (CDCl₃, 293 K) δ , ppm = -45.72 (major); -46.01, -46.84, -47.92 (minor).

cis 2:2 $Ru_2(amtfmp)_4(C_2Ph)_2$ (1). Phenylacetylene (0.15 mL, 1.4 mmol) was dissolved in 4.0 mL of THF, and the solution was degassed three times. This solution was then treated with 0.70 mL (1.8 mmol) of "BuLi at -78 °C and then allowed to reach room temperature. All of the alkynyllithium solution was added to a 50 mL solution of $Ru_2(amtfmp)_4Cl_2$ in THF (190 mg, 0.21 mmol), after which an immediate color change from blue to deep red was observed. The reaction mixture was stirred for 1 h under N_2 and after exposure to air turned a deep blue—green. After filtering over Celite and removing the solvent, the crude reaction mixture was purified with a silica plug run with 1:2 THF/hexanes with ca. 3% MeOH (v/v) to isolate 1 as a deep-blue solid. Compound 1 was recrystallized in a 1:1:25 THF/ethyl acetate (EtOAc)/hexanes (v/v) before EA.

Column chromatography (1:3 EtOAc/hexanes) was required to purify before electrochemical experiments. Single crystals suitable for X-ray diffraction were grown by layering hexanes over a concentrated solution of 1 in THF. Yield: 80 mg (36% based on Ru). TLC with 1:2 THF/hexanes with 3% methanol (v/v), $R_f = 0.64$. Elem. Anal. Found (calcd) for $C_{44}H_{34}N_8O_2F_{12}Ru_2$ (1·1EtOAc): C, 46.16 (46.48); H, 3.33 (3.01); N, 9.66 (9.86). ESI-MS $(m/z, based on ^{101}Ru)$: $[M]^+ =$ 1050. IR $\overline{\nu}/\text{cm}^{-1}$: 2090 $\overline{\nu}(\text{C}\equiv\text{C})$. UV-Vis (in THF) λ/nm ($\varepsilon/\text{M}^{-1}$ cm⁻¹): 452 (8300), 573 (8900), 619 (10000), 748 (4300). Electrochemistry (THF, vs Fc^{+/0}) $E_{1/2}/V$, $\Delta E_p/mV$, $i_{backward}/i_{forward}$: 0.619, irrev., -0.75 (62, 1.00), -1.81 (66, 0.96). ¹H NMR (CDCl₃, 293 K) δ , ppm = 9.64 (d, J = 6.0 Hz, 4H, H_A (amtfmp)), 9.43 (s, 4H, $H_{\rm R}$ (-NH)), 7.61-7.53 (m, 4H, $H_{\rm C}$ (amtfmp)), 7.33 (d, J = 4.4 Hz, 8H_. H_D (amtfmp/aryl)), 7.00–6.96 (m, 2H, H_E (aryl)), 6.68 (t, J =6.9 Hz, 4H, H_F (aryl)). ¹⁹F NMR (CDCl₃, 293 K) δ , ppm = -65.38. cis 2:2 $Ru_2(amtfmp)_4(C_6H_5)_2$ (**2**) and 3:1 $Ru_2(amtfmp)_4(C_6H_5)_2$ (**3**). Bromobenzene (0.50 mL, 4.8 mmol) was dissolved in 4.0 mL of THF and treated with 2.4 mL of ⁿBuLi (6.0 mmol) at 0 °C. The aryllithium solution was then cannula-transferred to a 70 mL solution of Ru₂(amtfmp)₄Cl₂ in THF (550 mg, 0.60 mmol). A color change from deep blue to red was observed. The reaction mixture was stirred for 1 h at room temperature and after exposure to air changed to purple. After filtering over Celite and removing the solvent, the crude product was purified via a silica plug run with 1:2 THF/hexanes with ca. 3%MeOH (v/v) to isolate 260 mg (33% combined yield based on Ru) of 2 and 3. From this plug, 220 mg of the starting material, Ru₂(amtfmp)₄Cl₂, was recollected (40% of the original starting material). The isomers were further purified by column chromatography. Two different product bands were eluted with 1:2 THF/ hexanes with ca. 3% MeOH (v/v), the front band red (2) and the back band purple (3). Compound 2 was recrystallized in a 1:1:25 THF/EtOAc/hexanes (v/v) before EA. Single crystals suitable for Xray diffraction were grown by layering hexanes over a concentrated solution of 2 in THF. Yield of 2: 95 mg (12% based on Ru). TLC with 1:2 THF/hexanes with 3% methanol (v/v), $R_f = 0.73$. Elem. Anal. Found (calcd) for C₄₄H₄₂N₈O₃F₁₂Ru₂ (2·1THF·1EtOAc): C₄ 45.50 (45.52); H, 3.45 (3.65); N, 9.35 (9.65). ESI-MS (m/z), based

 δ , ppm = -65.30. 3:1 $Ru_2(amtfmp)_4(C_6H_5)_2$ (3). Compound 3 was recrystallized in a 1:1:25 THF/EtOAc/hexanes (v/v) before EA. Single crystals suitable for X-ray diffraction were grown by layering hexanes over a concentrated solution of 3 in ethyl acetate. Yield of 3: 45 mg (7% based on Ru). TLC with 1:2 THF/hexanes with 3% methanol (v/v), $R_f = 0.70$. Elem. Anal. Found (calcd) for $C_{44}H_{44}N_8O_5F_{12}Ru_2$ (3. 2EtOAc·1H₂O): C, 44.11 (44.22); H, 3.91 (3.71); N, 9.04 (9.38). ESI-MS (m/z, based on ¹⁰¹Ru): [M + H]⁺ = 1001.8. UV–Vis (in THF) λ /nm (ε /M⁻¹ cm⁻¹): 415 (5900), 566 (7400), 710 (1000), 800 (700), 988 (270). Electrochemistry (THF, vs $Fc^{+/0}$) $E_{1/2}/V$, $\Delta E_{\rm p}/{\rm mV}$, $i_{\rm backward}/i_{\rm forward}$: 0.236 (59, 0.89), -1.01 (68, 1.00), -2.16 (66, 0.96). ¹H NMR (CDCl₃, 293 K) δ , ppm = 10.50 (s, 1H, H_A (-NH)), 9.62 (d, J = 6.6 Hz, 1H, H_B , (amtfmp)), 8.92 (d, J = 6.1 Hz, 1H, H_C , (amtfmp)), 8.59–8.41 (m, 2H, H_D , (amtfmp)), 7.84 (t, J =3.4 Hz, 1H, H_E , (-NH)), 7.54 (d, J = 7.4 Hz, 1H, H_E , (amtfmp)), 7.46 (t, J = 8.2 Hz, 2H, H_G, (amtfmp)), 7.36–7.29 (m, 4H, H_H, (aryl/ amtfmp)), 7.14 (t, J = 7.5 Hz, 2H, H_{ν} (amtfmp)), 6.99 (s, 2H, H_{ν} (-NH)), 6.84 (t, J = 6.9 Hz, 2H, H_K , (aryl)), 6.77 (t, J = 8.0 Hz, 1H, H_L , (amtfmp)), 6.61 (d, J = 7.8 Hz, 2H, H_M , (aryl)), 6.44 (t, J = 6.6Hz, 1H, H_N , (aryl)), 6.37 (t, J = 6.6 Hz, 1H, H_O , (aryl)), 6.00 (t, J =6.9 Hz, 2H, H_p, (aryl)). ¹⁹F NMR (CDCl₃, 293 K) δ , ppm = -64.55, -65.21, -65.62.

on 101 Ru): $[M + H]^+ = 1001.8$. UV-Vis (in THF) λ/nm ($\varepsilon/\text{M}^{-1}$

cm⁻¹): 433 (11300), 514 (6800), 573, (7800), 656 (2300), 710

(3700), 989 (190). Electrochemistry (THF, vs Fc^{+/0}) $E_{1/2}/V$, $\Delta E_p/$

mV, $i_{\text{backward}}/i_{\text{forward}}$: 0.31 (65, 0.97), -1.08 (66, 1.01), -2.10 (70,

1.13). ¹H NMR (CDCl₃, 293 K) δ , ppm = 9.17 (s, 4H, H_D (-NH)),

8.68 (d, J = 6.1 Hz, 4H, H_C (amtfmp)), 7.48 (d, J = 7.0 Hz, 4H, H_A

(amtfmp)), 7.28 (t, J = 6.0 Hz, 2H, H_B (amtfmp)), 7.24 (t, 2H, H_B

(amtfmp)), 7.09 (t, J = 7.6 Hz, 4H, H_E (aryl)), 7.02–6.96 (m, 2H, H_G (aryl)), 6.43 (t, J = 6.7 Hz, 4H, H_F (aryl)). ¹⁹F NMR (CDCl₃, 293 K)

X-ray Crystallographic Analysis. Single-crystal X-ray diffraction data for compound **2** at 150 K was collected on a Bruker AXS D8 Quest CMOS diffractometer using Mo-K α radiation (λ = 0.71073 Å). Single-crystal X-ray diffraction data for compounds **1** and **3** at 150 K were collected on a Bruker AXS D8 Quest CMOS diffractometer using Cu K α radiation (λ = 1.54178 Å). Data was collected and processed using APEX3⁵⁶ and SADABS,⁵⁷ and the structures were solved using the SHELXTL^{58,59} suite of programs and refined using Shelxl2018. ^{60,61}

Computational Methods. Geometry optimizations of structures 1 and 2 based on the respective crystal structures were done using restricted open-shell DFT; the B3LYP functional and lanl2dz basis set were used for all atoms⁶² in tetrahydrofuran. Frequency analyses were carried out for both the optimized structures 1' and 2', and stationary points were confirmed. All calculations were carried out using Gaussian 16, Rev. A.03.

ASSOCIATED CONTENT

Supporting Information

The Supporting Information is available free of charge at https://pubs.acs.org/doi/10.1021/acs.inorgchem.2c02498.

Additional crystallographic and computational details, absorption spectra and electrochemistry plots, $^1H/^{19}F$ NMR spectra, attempted synthesis of $Ru_2(amtfmp)_4Cl_2$ following the literature method, etc. (PDF)

Accession Codes

CCDC 2182912–2182914 contain the supplementary crystallographic data for this paper. These data can be obtained free of charge via www.ccdc.cam.ac.uk/data_request/cif, or by emailing data_request/cif, or by contacting The Cambridge Crystallographic Data Centre, 12 Union Road, Cambridge CB2 1EZ, UK; fax: +44 1223 336033.

AUTHOR INFORMATION

Corresponding Author

Tong Ren − Department of Chemistry, Purdue University, West Lafayette, Indiana 47907, United States; o orcid.org/ 0000-0002-1148-0746; Email: tren@purdue.edu

Authors

Lyndsy A. Miller-Clark — Department of Chemistry, Purdue University, West Lafayette, Indiana 47907, United States Peter E. Christ — Department of Chemistry, Purdue University, West Lafayette, Indiana 47907, United States Brian T. Barbarini — Department of Chemistry, Purdue University, West Lafayette, Indiana 47907, United States

Complete contact information is available at: https://pubs.acs.org/10.1021/acs.inorgchem.2c02498

Notes

The authors declare no competing financial interest.

ACKNOWLEDGMENTS

We gratefully acknowledge financial support from the National Science Foundation (CHE 1764347 and CHE 2102049). P.E.C. thanks the Department of Chemistry of Purdue University for an Undergraduate Summer Research Fellowship.

REFERENCES

- (1) Stephenson, T. A.; Wilkinson, G. New Ruthenium carboxylate Complexes. *J. Inorg. Nucl. Chem.* **1966**, *28*, 2285–2291.
- (2) Multiple Bonds between Metal Atoms, 3rd ed.; Cotton, F. A.; Murillo, C. A.; Walton, R. A., Eds.; Springer Science and Business Media, Inc.: New York, 2005.

- (3) Cortijo, M.; González-Prieto, R.; Herrero, S.; Priego, J. L.; Jiménez-Aparicio, R. The use of amidinate ligands in paddlewheel diruthenium chemistry. *Coord. Chem. Rev.* **2019**, *400*, 213040.
- (4) Van Caemelbecke, E.; Phan, T.; Osterloh, W. R.; Kadish, K. M. Electrochemistry of metal-metal bonded diruthenium complexes. *Coord. Chem. Rev.* **2021**, 434, 213706.
- (5) Handa, M.; Sayama, Y.; Mikuriya, M.; Nukada, R.; Hiromitsu, I.; Kasuga, K. A Chain Complex of Ruthenium(II,III) Cation Dimer Linked by a Nitroxide Radical, [Ru₂(O₂CCMe₃)₄(NITPh)]_n(NITPh-2-Phenyl-4,4,5,5-tetramethyl-4,5-dihydro-1*H*-imidazolyl-1-oxy-3-oxide). *Chem. Lett.* **1996**, 25, 201–202.
- (6) Sayama, Y.; Handa, M.; Mikuriya, M.; Hiromitsu, I.; Kasuga, K. Ferromagnetic Chain Complex of Ruthenium(II, III) Pivalate with Pyridyl Nitronyl Nitroxide. *Chem. Lett.* **1998**, *27*, 777–778.
- (7) Liao, Y.; Shum, W. W.; Miller, J. S. Synthesis and Magnetic Properties of 3-D [RuII/III2(O2CMe)4]3[MIII(CN)6] (M = Cr, Fe, Co). *I. Am. Chem. Soc.* **2002**, *124*, 9336–9337.
- (8) Vos, T. E.; Liao, Y.; Shum, W. W.; Her, J.-H.; Stephens, P. W.; Reiff, W. M.; Miller, J. S. Diruthenium Tetraacetate Monocation, [RuII/III2(O2CMe)4]+, Building Blocks for 3-D Molecule-Based Magnets. J. Am. Chem. Soc. 2004, 126, 11630–11639.
- (9) Miyasaka, H.; Clérac, R.; Campos-Fernández, C. S.; Dunbar, K. R. Metal-Metal Bonded Diruthenium(II, III) Assemblies with the Polycyano Anionic Linkers N(CN)2-, C(CN)3-, and 1,4-Dicyanamido-2,5-dimethylbenzene (DM-Dicyd2-): Syntheses, Structures, and Magnetic Properties. *Inorg. Chem.* **2001**, *40*, 1663–1671.
- (10) Barral, M. C.; Herrero, S.; Jiménez-Aparicio, R.; Torres, M. R.; Urbanos, F. A. A Spin-Admixed Ruthenium Complex. *Angew. Chem., Int. Ed.* **2005**, *44*, 305–307.
- (11) Barral, M. C.; Gallo, T.; Herrero, S.; Jiménez-Aparicio, R.; Torres, M. R.; Urbanos, F. A. Equatorially Connected Diruthenium-(II,III) Units toward Paramagnetic Supramolecular Structures with Singular Magnetic Properties. *Inorg. Chem.* **2006**, *45*, 3639–3647.
- (12) Komiya, N.; Nakae, T.; Sato, H.; Naota, T. Water-soluble diruthenium complexes bearing acetate and carbonate bridges: highly efficient catalysts for aerobic oxidation of alcohols in water. *Chem. Commun.* **2006**, 4829–4831.
- (13) Barker, J. E.; Ren, T. Diruthenium(II,III) Bis(tetramethyl-1,3-benzenedipropionate) As A Novel Catalyst for tert-Butyl Hydroperoxide Oxygenation. *Inorg. Chem.* **2008**, *47*, 2264–2266.
- (14) Corcos, A. R.; Pap, J. S.; Yang, T.; Berry, J. F. A Synthetic Oxygen Atom Transfer Photocycle from a Diruthenium Oxyanion Complex. J. Am. Chem. Soc. 2016, 138, 10032–10040.
- (15) Miyazawa, T.; Suzuki, T.; Kumagai, Y.; Takizawa, K.; Kikuchi, T.; Kato, S.; Onoda, A.; Hayashi, T.; Kamei, Y.; Kamiyama, F.; Anada, M.; Kojima, M.; Yoshino, T.; Matsunaga, S. Chiral paddle-wheel diruthenium complexes for asymmetric catalysis. *Nat. Catal.* **2020**, *3*, 851–858
- (16) Chakravarty, A. R.; Cotton, F. A. A New Diruthenium(II, III) Compound, Ru2(CCPh)(PhNpy)4.2CH2Cl2, with an Axial Acetylide Ligand. *Inorg. Chim. Acta* **1986**, *113*, 19–26.
- (17) Bear, J. L.; Han, B.; Huang, S. Molecular structure and electrochemistry of Ru2(dpf)4(C.tplbond.CC6H5)2 (dpf = N,N'-diphenylformamidinate ion): a novel ruthenium(III)-ruthenium(III) dimer. J. Am. Chem. Soc. 1993, 115, 1175–1177.
- (18) Bear, J. L.; Han, B.; Huang, S.; Kadish, K. M. Effect of Axial Ligands on the Oxidation State, Structure, and Electronic Configuration of Diruthenium Complexes. Synthesis and Characterization of Ru2(dpf)4Cl, Ru2(dpf)4(C:CC6H5), Ru2(dpf)4(C:CC6H5)2, and Ru2(dpf)4(CN)2 (dpf = N,N'-Diphenylformamidinate). *Inorg. Chem.* 1996, 35, 3012–3021.
- (19) Xu, G. L.; Zou, G.; Ni, Y. H.; DeRosa, M. C.; Crutchley, R. J.; Ren, T. Polyyn-diyls capped by diruthenium termini: A new family of carbon-rich organometallic compounds and distance-dependent electronic coupling therein. *J. Am. Chem. Soc.* **2003**, *125*, 10057–10065.
- (20) Ying, J.-W.; Liu, I. P.-C.; Xi, B.; Song, Y.; Campana, C.; Zuo, J.-L.; Ren, T. Linear Trimer of Diruthenium Linked by Butadiyn-Diyl

- Units: A Unique Electronic Wire. Angew. Chem., Int. Ed. 2010, 49, 954-957.
- (21) Xi, B.; Liu, I. P. C.; Xu, G.-L.; Choudhuri, M. M. R.; DeRosa, M. C.; Crutchley, R. J.; Ren, T. Modulation of Electronic Couplings within Ru2-Polyyne Frameworks. *J. Am. Chem. Soc.* **2011**, *133*, 15094–15104.
- (22) Cao, Z.; Xi, B.; Jodoin, D. S.; Zhang, L.; Cummings, S. P.; Gao, Y.; Tyler, S. F.; Fanwick, P. E.; Crutchley, R. J.; Ren, T. Diruthenium-Polyyn-diyl-Diruthenium Wires: Electronic Couplings in the Long Distance Regime. *J. Am. Chem. Soc.* **2014**, *136*, 12174—12183.
- (23) Miller-Clark, L. A.; Raghavan, A.; Clendening, R. A.; Ren, T. Phenylene as an efficient mediator for intermetallic electronic coupling. *Chem. Commun.* **2022**, *58*, 5478–5481.
- (24) Xu, G.-L.; Wang, C.-Y.; Ni, Y.-H.; Goodson, T. G.; Ren, T. Iterative Synthesis of Oligoynes Capped by A Ru2(*ap*)4-terminus and Their Voltammetric and Optoelectronic Properties. *Organometallics* **2005**, *24*, 3247–3254.
- (25) Blum, A. S.; Ren, T.; Parish, D. A.; Trammell, S. A.; Moore, M. H.; Kushmerick, J. G.; Xu, G.-L.; Deschamps, J. R.; Pollack, S. K.; Shashidhar, R. $Ru_2(ap)_4(\sigma-oligo(phenyleneethynyl))$ Molecular Wires: Synthesis and Electronic Characterization. *J. Am. Chem. Soc.* **2005**, *127*, 10010–10011.
- (26) Mahapatro, A. K.; Ying, J.; Ren, T.; Janes, D. B. Electronic Transport through Ruthenium Based Redox-Active Molecules in Metal-Molecule-Metal Nanogap Junctions. *Nano Lett.* **2008**, *8*, 2131–2136
- (27) Pookpanratana, S.; Zhu, H.; Bittle, E. G.; Natoli, S. N.; Ren, T.; Richter, C. A.; Li, Q.; Hacker, C. A. Non-volatile memory devices with redox-active diruthenium molecular compound. *J. Phys.: Condens. Matter* **2016**, *28*, 094009.
- (28) Zhu, H.; Pookpanratana, S. J.; Bonevich, J. E.; Natoli, S. N.; Hacker, C. A.; Ren, T.; Suehle, J. S.; Richter, C. A.; Li, Q. Redox-Active Molecular Nanowire Flash Memory for High-Endurance and High-Density Nonvolatile Memory Applications. *ACS Appl. Mater. Interfaces* **2015**, *7*, 27306–27313.
- (29) Ogawa, S.; Chattopadhyay, S.; Tanaka, Y.; Ohto, T.; Tada, T.; Tada, H.; Fujii, S.; Nishino, T.; Akita, M. Control of dominant conduction orbitals by peripheral substituents in paddle-wheel diruthenium alkynyl molecular junctions. *Chem. Sci.* **2021**, *12*, 10871–10877.
- (30) Su, S. D.; Zhu, X. Q.; Wen, Y. H.; Zhang, L. T.; Yang, Y. Y.; Lin, C. S.; Wu, X. T.; Sheng, T. L. A Diruthenium-Based Mixed Spin Complex Ru-2(5+)(S=1/2)-CN-Ru-2(5+)(S=3/2). *Angew. Chem., Int. Ed.* **2019**, *58*, 15344–15348.
- (31) Su, S.-D.; Zhu, X.-Q.; Wen, Y.-H.; Wu, X.-T.; Sheng, T.-L. Influence of Substitution Effect on MMCT in Mixed-Valence Cyanido-Bridged FeII-CN-Ru2III,III-NC-FeII System. *Eur. J. Inorg. Chem.* **2021**, 3474–3480.
- (32) Su, S.-D.; Wen, Y.-H.; Wu, X.-T.; Sheng, T.-L. Multiple MMCT properties of the diruthenium-based cyanido-bridged complex RuVI2-NC-RuII-CN-RuVI2. *Dalton Trans.* **2022**, *51*, 10047–10054.
- (33) Osterloh, W. R.; Galindo, G.; Yates, M. J.; Van Caemelbecke, E. V.; Kadish, K. M. Synthesis, Structural and Physicochemical Properties of Water-Soluble Mixed-Ligand Diruthenium Complexes Containing Anilinopyridinate Bridging Ligands. *Inorg. Chem.* **2020**, *59*, 584–594.
- (34) Li, Y.; Han, B.; Kadish, K. M.; Bear, J. L. A novel diamagnetic diruthenium(III) complex bridged by four unsymmetrical carboxylate-type ligands. Synthesis, molecular structure, electrochemistry, and spectroelectrochemistry of Ru2(pfap)4(C.tplbond.CC6H5)2, where pfap is 2,3,4,5,6-pentafluoro-2-anilinopyridinate. *Inorg. Chem.* 1993, 32, 4175–4176.
- (35) Xu, G.; Campana, C.; Ren, T. Tetrakis(*N*,*N*'-dimethylbenzamidinato)diruthenium Compounds Bearing Axial Chloro and Alkynyl Ligands: A New Family of Redox Rich Diruthenium Compounds. *Inorg. Chem.* **2002**, *41*, 3521–3527.
- (36) Xu, G.; Ren, T. Synthesis and characterization of transphenyethynylalkynyl adducts on a tetraanilinopyridinato-diruthenium-(III) core. *J. Organomet. Chem.* **2002**, *655*, 239–243.

- (37) Lin, C.; Ren, T.; Valente, E. J.; Zubkowski, J. D. Synthesis, spectroscopy and electrochemistry of tetrakis (μ -N, N '-diarylformamidinato) di(phenylethynyl) diruthenium (III). *J. Chem. Soc., Dalton Trans.* **1998**, 571–576.
- (38) Miller-Clark, L. A.; Christ, P. E.; Ren, T. Diruthenium aryl compounds tuning of electrochemical responses and solubility. *Dalton Trans.* **2022**, *51*, 580–586.
- (39) Raghavan, A.; Mash, B. L.; Ren, T. Forging Ru-Csp2 Bonds in Paddlewheel Complexes Using the Lithium-Halogen Exchange Reaction. *Inorg. Chem.* **2019**, *58*, 2618–2626.
- (40) Raghavan, A.; Ren, T. Bisaryl Diruthenium(III) Paddlewheel Complexes: Synthesis and Characterization. *Organometallics* **2019**, *38*, 3888–3896.
- (41) Kataoka, Y.; Mikami, S.; Sakiyama, H.; Mitsumi, M.; Kawamoto, T.; Handa, M. A neutral paddlewheel-type diruthenium-(III) complex with benzamidinato ligands: Synthesis, crystal structure, magnetism, and electrochemical and absorption properties. *Polyhedron* **2017**, *136*, 87–92.
- (42) Kataoka, Y.; Imasaki, N.; Arakawa, K.; Yano, N.; Sakiyama, H.; Sugimori, T.; Mitsumi, M.; Handa, M. Paddlewheel-type diruthenium(III, III) tetrakis(2-aminopyridinate) complexes with NIR absorption features: combined experimental and theoretical study. *Dalton Trans.* **2019**, *48*, 12421–12429.
- (43) Kataoka, Y.; Imasaki, N.; Yano, N.; Mitsumi, M.; Handa, M. Redox-triggered reversible modulation of intense near-infrared and visible absorption using a paddlewheel-type diruthenium(iii) complex. *Dalton Trans.* **2021**, *50*, 9547–9553.
- (44) Zou, G.; Alvarez, J. C.; Ren, T. Ru-σ-Alkynyl Compounds of Tetraanilinopyridinato-diruthenium(II,III) Core: Synthesis and Structural Characterization. *J. Organomet. Chem.* **2000**, *596*, 152–158.
- (45) Doyle, M. P.; Bagheri, V.; Wandless, T. J.; Harn, N. K.; Brinker, D. A.; Eagle, C. T.; Loh, K. L. Exceptionally high trans (anti) stereoselectivity in catalytic cyclopropanation reactions. *J. Am. Chem. Soc.* 1990, 112, 1906–1912.
- (46) Doyle, M. P.; Winchester, W. R.; Hoorn, J. A. A.; Lynch, V.; Simonsen, S. H.; Ghosh, R. Dirhodium(II) tetrakis(carboxamidates) with chiral ligands. Structure and selectivity in catalytic metal-carbene transformations. *J. Am. Chem. Soc.* **1993**, *115*, 9968–9978.
- (47) Kadish, K. M.; Wang, L.-L.; Thuriere, A.; Van Caemelbecke, E. V.; Bear, J. L. Factors Affecting the Electrochemical and Spectroelectrochemical Properties of Diruthenium(III,II) Complexes Containing Four Identical Unsymmetrical Bridging Ligands. *Inorg. Chem.* 2003, 42, 834–843.
- (48) Bear, J. L.; Li, Y.; Han, B.; Van Caemelbecke, E. V.; Kadish, K. M. Isomer Effect on the Structure and Chemical Reactivity of Diruthenium Complexes. Synthesis and Characterization of the (4,0), (3,1), and (2,2) Trans Isomers of $\mathrm{Ru}_2(\mathrm{F}_5\mathrm{ap})_4\mathrm{Cl}$ and $\mathrm{Ru}_2(\mathrm{F}_5\mathrm{ap})_4(\mathrm{CCPh})_2$ Where $\mathrm{F}_5\mathrm{ap}$ Is the 2-(2,3,4,5,6-Pentafluoroanilino)pyridinate Anion. *Inorg. Chem.* 1997, 36, 5449–5456
- (49) Nguyen, M.; Phan, T.; Caemelbecke, E. V.; Kajonkijya, W.; Bear, J. L.; Kadish, K. M. Interconversion between (3,1) and (4,0) Isomers of Ru2(L)4X Complexes where L is 2-Anilinopyridinate or 2-(2,4,6-Trifluoroanilino)pyridinate Anion and X = Cl- or C=CC5H4N-. *Inorg. Chem.* **2008**, *47*, 7775–7783.
- (50) Bear, J. L.; Chen, W.-Z.; Han, B.; Huang, S.; Wang, L.-L.; Thuriere, A.; Van Caemelbecke, E. V.; Kadish, K. M.; Ren, T. Cyanide Adducts on the Diruthenium Core of [Ru2(L)4]+(L=ap, CH3ap, Fap or F3ap) as Potential Supramolecular Synthons. Electronic Properties and Binding Symmetry of the Bridging Ligand. *Inorg. Chem.* **2003**, 42, 6230–6240.
- (51) Hurst, S. K.; Xu, G.-L.; Ren, T. *Bis*-Adducts of Substituted Phenylacetylide on a Ru2(DMBA)4 Core: Effect of Donor/Acceptor Modifications. *Organometallics* **2003**, *22*, 4118–4123.
- (52) Ren, T. Diruthenium σ-Alkynyl Compounds: A New Class of Conjugated Organometallics. *Organometallics* **2005**, 24, 4854–4870.
- (53) Ren, T. Dissymmetrical *trans*-Ethynyl-Butadiynyl Adducts on A Diruthenium Core: Synthesis, Characterization and Selective Deprotection. *Organometallics* **2002**, *21*, 732–738.

- (54) Kadish, K. M.; Phan, T. D.; Wang, L.-L.; Giribabu, L.; Thuriere, A.; Wellhoff, J.; Huang, S.; Caemelbecke, E. V.; Bear, J. L. Synthesis, Structural, Spectroscopic, and Electrochemical Characterization of High Oxidation State Diruthenium Complexes Containing Four Identical Unsymmetrical Bridging Ligands. *Inorg. Chem.* **2004**, *43*, 4825–4832.
- (55) Manna, J.; John, K. D.; Hopkins, M. D. The Bonding of Metal-Alkynyl Complexes. *Adv. Organomet. Chem.* **1995**, *38*, 79–154.
- (56) Bruker. Apex3 v2016.9-0, Saint V8.34A, Saint V8.37A; Bruker AXS Inc.: Madison, WI, 2016.
- (57) Krause, L.; Herbst-Irmer, R.; Sheldrick, G. M.; Stalke, D. Comparison of silver and molybdenum microfocus X-ray sources for single-crystal structure determination. *J. Appl. Crystallogr.* **2015**, 48, 3–10.
- (58) SHELXTL, Version 6.14; Bruker Advanced X-ray Solutions, Bruker AXS Inc.: Madison, WI, 2000–2003.
- (59) Sheldrick, G. M. A short history of SHELX. Acta Crystallogr. 2008, 64, 112–122.
- (60) Sheldrick, G. M. SHELXL 2018; University of Göttingen: Germany. 2018.
- (61) Sheldrick, G. M. Crystal structure refinement with SHELXL. Acta Crystallogr., Sect. C: Struct. Chem. 2015, 71, 3–8.
- (62) Parr, R. G. Density Functional Theory of Atoms and Molecules; Oxford University Press: New York, 1989.
- (63) Frisch, M. J.; Trucks, G. W.; Schlegel, H. B.; Scuseria, G. E.; Robb, M. A.; Cheeseman, J. R.; Scalmani, G.; Barone, V.; Petersson, G. A.; Nakatsuji, H.; Li, X.; Caricato, M.; Marenich, A. V.; Bloino, J.; Janesko, B. G.; Gomperts, R.; Mennucci, B.; Hratchian, H. P.; Ortiz, J. V.; Izmaylov, A. F.; Sonnenberg, J. L.; Williams-Young, D.; Ding, F.; Lipparini, F.; Egidi, F.; Goings, J.; Peng, B.; Petrone, A.; Henderson, T.; Ranasinghe, D.; Zakrzewski, V. G.; Gao, J.; Rega, N.; Zheng, G.; Liang, W.; Hada, M.; Ehara, M.; Toyota, K.; Fukuda, R.; Hasegawa, J.; Ishida, M.; Nakajima, T.; Honda, Y.; Kitao, O.; Nakai, H.; Vreven, T.; Throssell, K.; Montgomery, J. J. A.; Peralta, J. E.; Ogliaro, F.; Bearpark, M. J.; Heyd, J. J.; Brothers, E. N.; Kudin, K. N.; Staroverov, V. N.; Keith, T. A.; Kobayashi, R.; Normand, J.; Raghavachari, K.; Rendell, A. P.; Burant, J. C.; Iyengar, S. S.; Tomasi, J.; Cossi, M.; Millam, J. M.; Klene, M.; Adamo, C.; Cammi, R.; Ochterski, J. W.; Martin, R. L.; Morokuma, K.; Farkas, O.; Foresman, J. B.; Fox, D. J. Gaussian 16, Revision A 03; Gaussian, Inc.: Wallingford, CT, 2016.

☐ Recommended by ACS

Electronic Structure of Ru₂⁶⁺ Complexes with Electron-Rich Anilinopyridinate Ligands

Michael D. Roy, John F. Berry, et al.

FEBRUARY 17, 2022

READ 🗹

Doublet Ground State in a Vanadium(II) Complex: Redox and Coordinative Noninnocence of Tripodal Ligand Architecture

Justin P. Joyce, Matthew P. Shores, et al.

APRIL 15, 2022

INORGANIC CHEMISTRY

READ 🗹

pH- and Time-Dependent Release of Phytohormones from Diruthenium Complexes

Isabel Coloma, Santiago Herrero, et al.

MAY 15, 2020

INORGANIC CHEMISTRY

RFAD **[**✓

Synthesis, Characterization, and Electrochemistry of Copper Dibenzoporphyrin(2.1,2.1) Complexes

Ningchao Liu, Songlin Xue, et al.

FEBRUARY 15, 2022

INORGANIC CHEMISTRY

READ 🗹

Get More Suggestions >